Available online at www.sciencedirect.com

ScienceDirect

journal homepage: www.elsevier.com/locate/he

Enhancement of visible light-driven hydrogen production over zinc cadmium sulfide nanoparticles anchored on $BiVO_4$ nanorods

Muhammad Imran [a,1], *Ammar Bin Yousaf* [b,1], *Muhammad Farooq* [c,d,**], *Peter Kasak* [b,*]

[a] *Hefei National Laboratory for Physical Sciences at Microscale, University of Science and Technology of China, Hefei, Anhui, 230026, PR China*

[b] *Center for Advanced Materials, Qatar University, P. O. Box 2713, Doha, Qatar*

[c] *Department of Chemistry, University of Management and Technology, Lahore, 54000, Pakistan*

[d] *Department of Chemistry and Materials, Faculty of Textile Science and Technology, Shinshu University, Ueda, 386-8567, Japan*

HIGHLIGHTS

- A novel $BiVO_4$–ZnCdS heterostructure is introduced as photocatalyst.
- The developed catalyst was used for visible light driven hydrogen production.
- Interface among $BiVO_4$ and ZnCdS improved photocatalytic profile of catalyst.
- $BiVO_4$–ZnCdS heterostructure produced up to 152.5 μmol g^{-1} h^{-1} hydrogen.
- Z-scheme mechanism enhanced the performance herein as noble-metal-free catalyst.

GRAPHICAL ABSTRACT

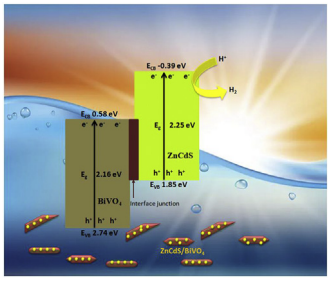

ARTICLE INFO

Article history:
Received 4 November 2021
Received in revised form
19 December 2021
Accepted 21 December 2021
Available online 20 January 2022

ABSTRACT

Photocatalytic water splitting to produce H_2 is a promising technology for clean energy generation. However, the use of expensive noble metals, toxicity, low charge separation efficiency and wide band gap of semiconductors hampering the widespread commercialization. Herein, we showed the potential of combining $BiVO_4$ nanorods with ZnCdS forming a hetero-structure which extend the spectral responsive range, separate the charge carriers effectively and enhances photocatalytic activity compared to single-component materials. The two components of hetero-structure forms an interface contact which also mitigate

* *Corresponding author.*
** *Corresponding author.* Department of Chemistry, University of Management and Technology, Lahore 54000, Pakistan.
E-mail addresses: mufaroouk@gmail.com, 20hs109g@shinshu-u.ac.jp (M. Farooq), peter.kasak@qu.edu.qa (P. Kasak).
[1] These two authors contributed equally.

https://doi.org/10.1016/j.ijhydene.2021.12.193

Keywords:
$BiVO_4$–ZnCdS
Heterostructure
H_2 production
Water splitting
Z-scheme

the problems of lower conduction band position of $BiVO_4$ and fast recombination of charge carriers of ZnCdS. The $BiVO_4$–ZnCdS hetero-structure was studied through surface morphology, crystallization properties, elemental analysis and optical properties. Under visible light irradiation, the $BiVO_4$–ZnCdS heterostructure produced 152.5 μmol g^{-1} h^{-1} hydrogen from water splitting, which was much higher than that of the individual components and stability of the hydrogen production was observed in three consecutive cycles. The as-obtained heterostructure showed improved visible light harvesting ability, prolong life of charges carriers and charge separation efficiency and Z-scheme mechanism features which results in enhanced photocatalytic activity for water splitting.

Introduction

Clean and renewable energy resources are one of the top priorities for future generations to meet the growing global energy demands due to depleting fossil fuel reserves and global warming threats [1]. During last few decades, number of strategies has been praised for clean energy production including fuel cells, water splitting and solar energy harvesting [2]. Water splitting to produce H_2 is a promising clean energy technology and has attracted major attention from broad spectrum of researchers after the initial work by Fujishima and Honda in 1972 [3]. As the core concept is based on solar light driven reaction, photocatalysis jumped in as auspicious choice for hydrogen production using photocatalyst and sacrificial agent operating under ambient conditions which can be applied at scalable levels with better recycling capabilities [4–6]. The characteristics of a suitable photocatalyst for hydrogen production depend on its band gap profile as wide band gap materials only utilize ultraviolet (UV) portion of light which constitute only a small fraction of incoming solar light [7–10]. Thus, the higher tendency to absorb visible light portion from solar light proportionally correlate with enhanced performance of photocatalyst for hydrogen production [11,12]. In addition, the higher charge separation efficiency, good redox capability and greater stability also joins the key features of excellent photocatalysts. In order to combine all these exceptional characteristics, heterostructure based catalysts proved to be a better choice than that of single component system due to enhanced flexibility in modifying the structure [13,14]. Recent theoretical principles studies, reaction mechanism and kinetic studies also shows the importance of heterostructure based catalysts compared to single component [15,16].

Cadmium sulfide (CdS) with band gap of 2.4 eV have been considered a better choice for H_2 production that have tendency to absorb greater fraction of visible light from irradiated solar light. However, the fast recombination of charge carriers and photo-corrosion issues of CdS negatively affects its practical long-term implementation [17]. To handle with this drawback, intermixing CdS with ZnS constituting a ZnCdS hetero-structure geometry have proved to positively affect the characteristics of catalyst in a dual pathway i.e., improves its resistance towards photo-corrosion and also improves the visible light absorption ability [18,19]. However, it was observed that the CdS component in ZnCdS deteriorates over a period of time resulting in decreased photocatalytic performance which also lower recyclability. While scratching the fate of photocatalysts, it has also been found that bismuth and vanadium oxides individually proved themselves in photocatalytic dye-degradation reactions as heterogeneous catalyst in visible light driven processes due to their good photoconductivities, photo-luminescence and redox properties [20–22]. It has also been observed that bismuth vanadate ($BiVO_4$) can serve as a potential photocatalyst for its advantages of narrow band gap, low cost and good stability [23]. However, its poor adsorption performance and difficulty in migration and separation of electron-hole pairs and lowers conduction band position hinders its application for hydrogen production [24]. To resolve these problems, $BiVO_4$ is usually coupled with another semiconductor forming a heterostructure based photocatalysts which improves the charge separation efficiency and enhances photocatalytic performance. Recent studies have shown the potential of combining $BiVO_4$ with other semiconductors such as g-C_3N_4, WO_3 and Pt–/TiO_2 for photocatalytic applications. However, these heterostructure combinations could not provide desired results as few of them may work better in the presence of precious metal co-catalyst which strongly hinders its economical standards while others show low performance [25–27]. Alternatively, another strategy of heterostructure combinations called "Z-scheme water-splitting system" is rapidly gaining interests, H_2 and O_2 evolving photocatalysts are combine together to form heterostructure, which follows Z-scheme charge transfer mechanism similar to natural photosynthesis [28]. There are many reports about use of different combinations for Z-scheme photocatalysis such as H_xMoO_3@$ZnIn_2S_4$, WO_3/g-C_3N_4, $Bi_4O_5Br_2$/g-C_3N_4, g-C_3N_4/Ag_2CrO_4 and Pt/GaP-TiO_2-SiO_2:Rh. However, usually a charge carrier transfer mediator is required which lowers photocatalytic performance owing to the shielding effect and high cost or overall performance is not satisfactory [29–34]. In addition, to achieve superior solar light utilization efficiency, the developed photocatalysts should feature a wide light response range, and simultaneously, should produce the charge carriers with suitable energy levels for implementing the specific photocatalytic redox processes. Thus, the selection of suitable semiconductors with appropriate band structures is a prerequisite for successful fabrication of direct Z-scheme photocatalysts.

Herein, we have introduced $BiVO_4$–ZnCdS heterostructure based on Z-scheme electron and hole transportation mechanism. In particular, owing to the strong visible light absorption and proper energy band level of ZnCdS, the $BiVO_4$–ZnCdS heterostructure could effectively utilize solar energy for photocatalytic application. Moreover, the problems of lower conduction band position of $BiVO_4$ and photocorrosion ability of CdS are successfully mitigated. The combination results in an interface contact between $BiVO_4$ and ZnCdS to enables a Z-scheme type pathway which enhances the performance of photocatalyst by facilitating the electrons transfer phenomenon, enabling the efficient charge separation and improving the stability of photocatalysts.

Experimental

Chemicals

Bismuth(III) nitrate pentahydrate [$Bi(NO_3)_3.5H_2O$], ammonium metavanadate (NH_4VO_3), nitric acid (HNO_3), sodium hydroxide (NaOH), zinc acetate [$Zn(OAc)_2$], cadmium acetate [$Cd(OAc)_2$], sodium sulfide nonahydrate [$Na_2S{\cdot}9H_2O$], sodium sulfite (Na_2SO_3) were of analytical grade and used as received without further purification.

Characterization

The structure and morphology of prepared sample was measured through transmission electron microscope, high-resolution transmission electron microscope and high-angle annular dark-field scanning transmission electron microscope (JEM-2100F, 200 kV accelerating voltage) with EDX elemental mapping. The crystal phase of samples was measured by powder X-ray diffraction (XRD) measurements with Philips X'Pert Pro Super diffractometer with Cu-Kα radiation ($\lambda = 1.54178$ Å) at operating voltage of 40 kV and current at 200 mA. The scanning angle range was set from 10 to 80°. The elemental composition of the prepared catalyst was performed using X-ray photoelectron spectroscopy (XPS) analysis (PerkinElmer RBD). The UV–vis diffuse reflectance spectra for band gap calculation and absorption behavior were recorded with Shimadzu spectrophotometer (2501 PC model) in the region of 200–800 nm.

Preparation of $BiVO_4$ nanorods

The $BiVO_4$ nanorods were prepared using following protocol; In a typical synthesis, equimolar amounts of $Bi(NO_3)_3{\cdot}5H_2O$ and NH_4VO_3 were dissolved in 2 M aq. HNO_3 solution. The pH of the mixed solution was adjusted to ~7.0 using ethylenediamine and subsequently the mixture was heat treated in Teflon-lined stainless-steel autoclave at 150 °C for 6 h. The obtained powders were separated with centrifugation, washed several times with MQ water and ethanol and dried at 60 °C in vacuum oven.

Preparation of $BiVO_4$–ZnCdS heterostructure

The heterostructure of $BiVO_4$ and ZnCdS was prepared using our previous protocol [35] described briefly as; $BiVO_4$ nanorods were first dispersed in deionized water, then appropriate amount of $Zn(OAc)_2$ and $Cd(OAc)_2$ were added into the dispersion to get a 10 wt% of ZnCdS onto $BiVO_4$ nanorods. Afterwards, pH of the mixture was adjusted to ~7.0 with dilute aqueous sodium hydroxide. Aqueous sodium sulfide solution was subsequently added into the mixture and stirred at room temperature for overnight. The samples were collected through centrifugation, washed with water and ethanol and dried in vacuum oven at 60 °C overnight. Finally, the obtained powders were calcined for 2 h at 400 °C under nitrogen flow with a heating rate of 5 °C/min.

Photocatalytic activity test

Hydrogen production under visible light over as-synthesized samples was performed using vacuumed closed cell circulation system equipped with 300 W Xe lamp and a cut-off filter to block the ultraviolet light ($\lambda \geq 420$ nm). The as-prepared catalysts (100 mg) were dispersed in MQ water (100 mL) containing sodium sulfide (0.25 M) and sodium sulfite (0.35 M), which act as sacrificial agents. Agilent 6820 gas chromatograph system was attached with the apparatus to measure the amount of hydrogen produced during the reaction.

Electrochemical and photo-electrochemical measurements

Photoelectrochemical tests were performed at CHI 660B electrochemical potentiostat (Chenhua Instrument Co., Shanghai, China) with three-electrode setup (modified Ti foil as working electrode, Ag/AgCl as reference electrode, and Pt wire as counter electrode) in 0.1 M Na_2SO_4 solution. The catalysts films were prepared by dropping catalyst suspension onto Ti foil (1 cm^2) and heated at 100 °C for overnight. The amperometric photocurrents were observed by switch on/off with a bias voltage of 0.5 V under visible-light. The electrochemical impedance spectroscopy (EIS) was recorded with −0.6 V bias and the frequency ranged from 1 Hz to 100 kHz with an alternating current signal amplitude of 5 mV.

Results and discussion

The morphological features and size of as-synthesized $BiVO_4$ nanorods, ZnCdS nanoparticles and $BiVO_4$–ZnCdS heterostructure was studied by Scanning electron microscope (SEM) (Fig. 1). As-shown in Fig. 1A, the $BiVO_4$ photocatalyst material is of rod shape ranging in size from 200 to 300 nm in diameter and about 1 μm in length. No other shape structures were observed indicating the successful synthesis of nanorods. Fig. 1B shows as-prepared ZnCdS sample which are mostly irregular shaped nanoparticles with about 10–20 nm in diameter. After depositing ZnCdS nanoparticles onto $BiVO_4$ nanorods, a composite of $BiVO_4$–ZnCdS heterostructure can be seen in Fig. 1C and D. The ZnCdS nanoparticles are successfully loaded onto the BiVO4 nanorods and a composite type structure can be seen. Transmission electron microscopy (TEM) analysis at different magnifications was also used to characterize the as-synthesized $BiVO_4$–ZnCdS heterostructure as shown in Fig. 2A–C. Presented in Figs. 2A & 1B, the desired catalyst material was successfully synthesized with nanorods of $BiVO_4$ fabricated with

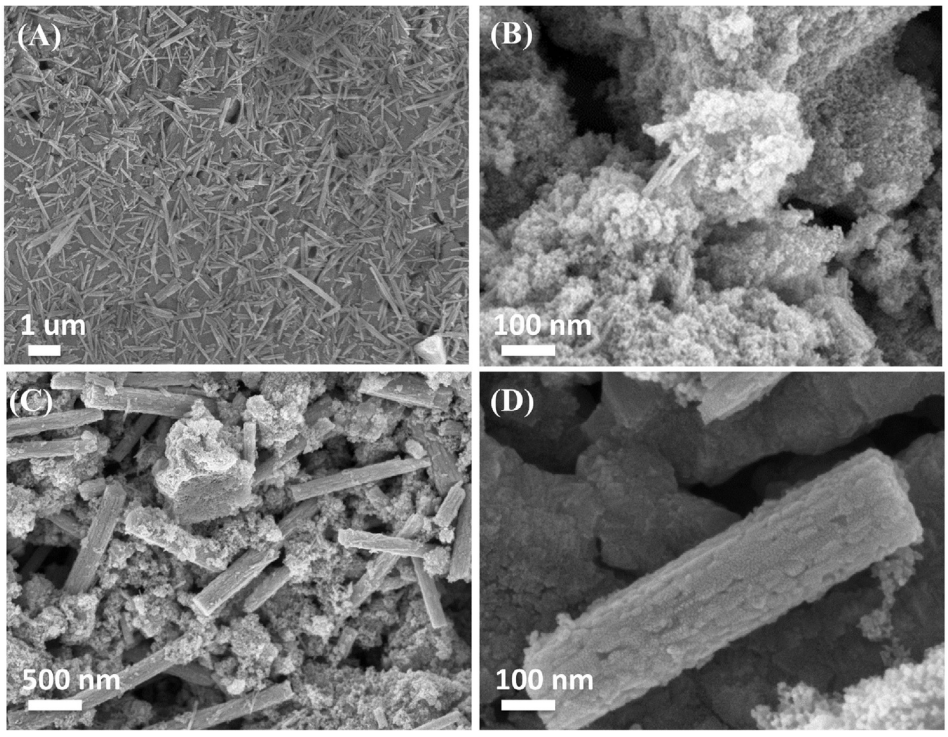

Fig. 1 – (A) SEM image for as-prepared $BiVO_4$ nanorods, (B) SEM image ZnCdS nanoparticles, (C) SEM image of $BiVO_4$–ZnCdS sample at low resolution, (D) SEM image of $BiVO_4$–ZnCdS sample at high resolution.

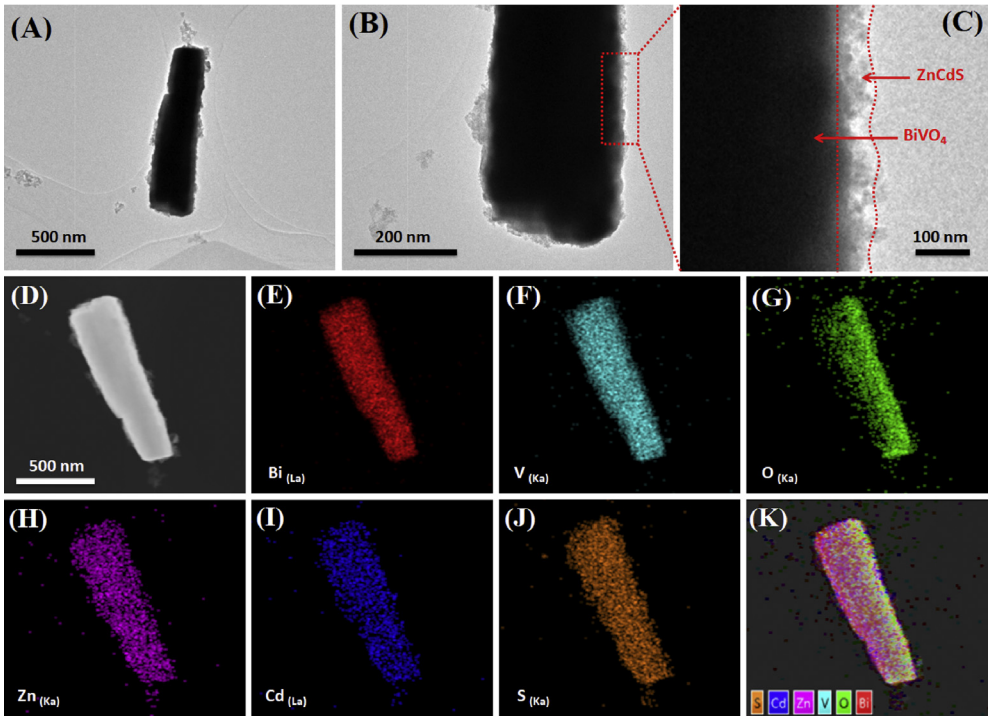

Fig. 2 – (A) TEM image for as-prepared $BiVO_4$–ZnCdS sample at lower magnifications, (B & C) TEM images for $BiVO_4$–ZnCdS sample at higher magnifications. (D) selected area for SAAED element mapping for $BiVO_4$–ZnCdS sample, (E–J) SAEED element mapping images for individual elements i-e Bi, V, O, Zn, Cd & S, respectively, (K) overlay image for element mapping.

nano-sized ZnCdS nanoparticles on their surface. The characteristic presence of ZnCdS nanoparticles on the surface of $BiVO_4$ is presented in Fig. 2C taken from the selected face side of the hetero-structured material. The hetero-junction catalyst material can also be proved with drawn red dotted lines in Fig. 2C differentiating two different components within hetero-structured material. As the fabricated ZnCdS nanoparticles dispersed thoroughly on the surface of $BiVO_4$, it was important to evaluate the homogeneity of different component-based catalyst material by elemental mapping analysis. The HAADF-STEM elemental mapping analysis also confirmed the homogeneous dispersion of each metal within the defined structure of material. Shown in Fig. 2D & E-J, the selected area of heterostructured material for the scan of individual elements and element mapping images for each metal enclosed in catalyst material, respectively. The overlay image for combined element mapping images presented in Fig. 2K also suggested the uniform dispersion of Bi, V & O forming the $BiVO_4$ and similarly Zn, Cd & S composing ZnCdS nanoparticles, thereby obtaining the overall homogenous $BiVO_4$–ZnCdS hetero-structure material. This homogeneity in morphology analysis may further support the metal-to-metal interactions for transference of electrons and better ductile behavior required for photocatalytic hydrogen production task.

The crystallite structure of $BiVO_4$–ZnCdS hetero-structure was analyzed by X-ray diffraction (XRD) technique. The characteristic XRD features of $BiVO_4$–ZnCdS were critically examined by comparing the individual XRD spectra of $BiVO_4$ and ZnCdS both the components with that of final hetero-structured material, shown in Fig. 3. While analyzing the obtained XRD spectrum of ZnCdS, it has been found that the planes (111), (220) and (311) of cubic Zinc blend phase (ICSD # 80–0020) indexed at 27.34°, 45.32° and 53.66°, respectively, indicate the formation of ZnCdS nanoparticles [35,36]. Whereas, the $BiVO_4$ XRD spectrum contains the characteristic featured peaks of both monoclinic (ICSD # 100,602) and tetragonal (ICSD # 100,733) phases of $BiVO_4$. The monoclinic phase of $BiVO_4$ is a binary equivalents crystal structure consist of a layered structure of V_2O_5 and Bi_2O_3. In accordance with $BiVO_4$, no additional peaks related to impurities were detected [37,38]. The XRD spectra of $BiVO_4$–ZnCdS heterostructure contains all characteristics peaks corresponding to $BiVO_4$. However, the diffraction peaks of ZnCdS in the $BiVO_4$–ZnCdS heterostructure were not prominent, likely due to the low content and smaller particle size. In order to provide critical analysis, for intermixed lattice of ZnCdS nanoparticles fabricated on the surface of $BiVO_4$, the variation in specific peaks intensities and minor shift was noticed. The shift in XRD peak position may indicate that the crystal structure of $BiVO_4$ nanorods influenced by ZnCdS nanoparticles most probably due to interaction of Zn–Cd–S ions with $BiVO_4$. The interaction may cause structural distortions within the nanostructure which produces lattice strains resulting in peak shift [39]. These investigations strongly confirm the successful synthesis of $BiVO_4$–ZnCdS hetero-structured catalyst based on its crystallographic analysis.

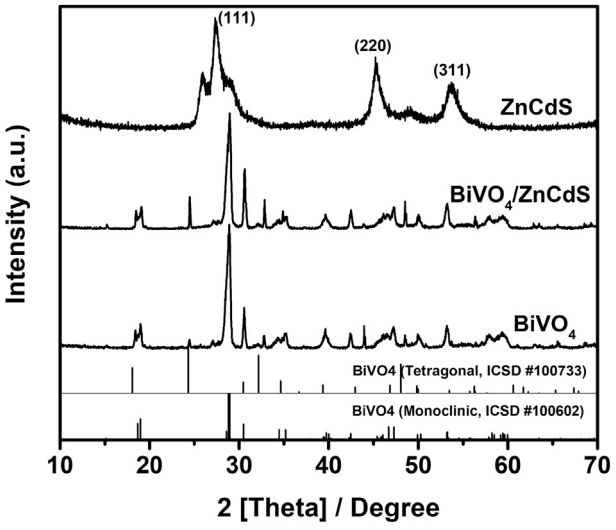

Fig. 3 – XRD spectrum for $BiVO_4$–ZnCdS sample in comparison with $BiVO_4$ and ZnCdS spectra and standard for monoclinic and tetragonal phases of $BiVO_4$.

The structural analysis of $BiVO_4$–ZnCdS was further investigated by means of X-ray photoelectron spectroscopy (XPS) to extend and strengthen the proof of synthesis. The full survey scan of XPS was appeared with well-indexed characteristic peaks of each element in $BiVO_4$–ZnCdS material (i-e Bi, V, O, Zn, Cd & S) positioned at their respective standard and documented binding energies values, shown in Fig. S1 [40,41]. Furthermore, the high resolution XPS scan of Bi (4f) typically owned two doublets correspond to Bi $(4f)_{5/2}$ and Bi $(4f)_{7/2}$ at binding energy values of 164.26 eV and 158.97 eV, respectively, shown in Fig. 4A. In comparison with reported binding energy values of Bi (4f) domains, it has been noticed the up-shift in binding energies of 0.49 eV in Bi $(4f)_{5/2}$ and up-shift of 0.50 eV in Bi $(4f)_{7/2}$ happened. The high resolution XPS scan of V (2p) signals are orbit splitting into V $(2p)_{1/2}$ and V $(2p)_{3/2}$ at binding energy values of 524.13 eV and 516.58 eV, respectively [42], shown in Fig. 4B. The shift in their binding energies towards higher values were indexed compared from standard and documented values of V (2p). This shift in binding energy towards higher binding energy values suggests the change in chemical environment due to effective charge transfer between $BiVO_4$ and ZnCdS components indicating a strong interaction in heterostructure composite [40,43]. The O (1s) spectrum showed two peak proportions located at 529.68 eV and 531.43 eV for characteristic features of lattice oxygen and surface adsorbed oxygen coupled with water and CO_2 in form of O–H and O–C groups (Fig. 4C). The O1s spectra can be further deconvoluted into Gaussian curves. The low-binding-energy component is ascribed to the O^{2-} ions in $BiVO_4$, while the component in the higher-binding-energy region is related to the physisorbed water molecules and carbon components [43]. The XPS high resolution scan of O (1s) also suggesting that the adsorbed oxygen atoms on the surface of catalyst may behave as captive of photogenerated electron-hole pairs in a direct way that can also inhibit further photogenerated electron-hole recombination. This phenomenon may also enhance the lifetime of these photogenerated carriers, thereby increasing the quantum efficiency of catalyst for enhanced photocatalytic performance [43]. The high resolution XPS spectrum of Zn (2p) and Cd (3d) contain spin-orbit components such as, Zn $(2p_{3/2})$ & Zn $(2p_{1/2})$ indexed at

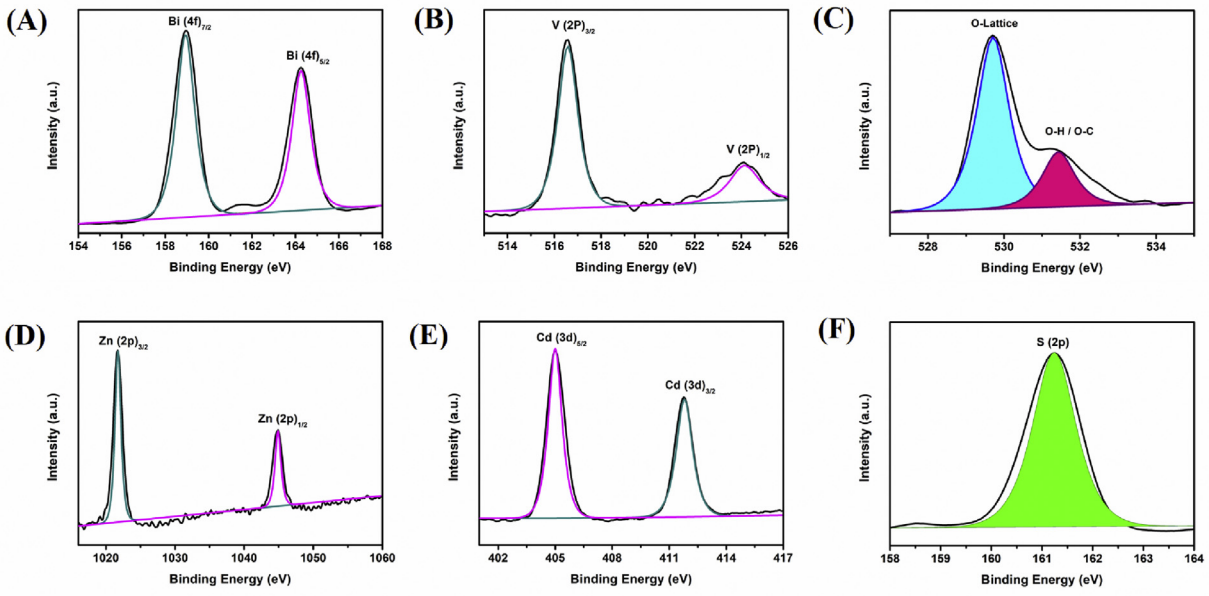

Fig. 4 – XPS high resolution scans for (A) Bi 4f, (B) V 2p, (C) O 1S, (D) Zn 2p, (E) Cd 3d and (F) S 2p.

1021.81 eV & 1045.09 eV, respectively, and Cd ($3d_{5/2}$) & Cd ($3d_{3/2}$) at binding energy values of 404.97 eV & 411.80 eV, respectively, shown in Fig. 4D & E. The obtained XPS peaks existences and positions for Zn (2p) and Cd (3d) are well agreed with the values literature values of divalent Zn and Cd present in pure metal sulphides molecules. The S (2p) high resolution spectra show a peak proportion at 161.29 eV which can be ascribed to S^{2-} valent state of S in ZnCdS component of $BiVO_4$–ZnCdS material, shown in Fig. 4F [41]. The smaller difference in obtained binding energy values for Zn, Cd and S was observed from that of standard values in $BiVO_4$–ZnCdS which may correlate with the difference in valence electron density and relaxation energy by intimate contact of ZnCdS with $BiVO_4$ in $BiVO_4$–ZnCdS material.

The absorption properties (UV–visible absorption) of semiconductor's can be used as a precursor to investigate the material's photocatalytic performance and band gap calculations which gives an approximation of photocatalyst's ability to generate electrons and holes under visible light illumination [44]. The as-prepared $BiVO_4$ nanorods, Zinc-cadmium sulfide nanoparticles and $BiVO_4$–ZnCdS hetero-structured catalysts were characterized with UV–visible diffuse reflectance spectra to observe the optical properties. As shown in Fig. 5A, the $BiVO_4$ nanorods shows absorption in the visible-light region which can be ascribed to the light illuminated electron's excitation to Vanadium 3d orbital from Bismuth 6s and Oxygen 2p orbitals [45]. The ZnCdS nanoparticles also shows strong absorption characteristics due to movement of free electrons from the conduction band to a higher Fermi level. However, the absorption edge shows red shift towards higher wavelength indicating stronger absorption in the visible region due to low band gap of CdS component and less energy requirement for excitation of free electrons. The as-synthesized $BiVO_4$–ZnCdS heterostructure on the other hand with a darker color displays strong visible light absorption compared to bare samples indicating the superior visible light response which could significantly improve photocatalytic hydrogen production. The visible-light absorption of semiconductors are related to the electronic structure and band alignment and band gap values can be calculated from UV–visible diffuse reflectance spectra using Tauc formula $\alpha h\nu = A(h\nu - E_g)^{n/2}$ [46] where α is the absorption coefficient, h is the Planck constant, and ν is the optical frequency; A is a constant and E_g is the band gap. Fig. 5B shows the *Tauc* plots and calculated corresponding band gap energies obtained from the intercept of the tangent of the curve of $(\alpha h\nu)^2$*versus* $(h\nu)$ on the X-axis. The band gap energies for $BiVO_4$ nanorods, ZnCdS nanoparticles and $BiVO_4$–ZnCdS heterostructure calculated to be 2.16 eV, 2.25 eV and 2.02 eV respectively. The values for $BiVO_4$ and ZnCdS are in close approximation to the literature values indicating successful synthesis of the catalysts [47,48]. The band gap energy value for $BiVO_4$–ZnCdS heterostructure also strongly indicate strong visible light absorption characteristics which might help in enhancing the photocatalytic performance. The change in band gap after combining heterostructure also indicate the structural distortions within the nanostructure which produces lattice strains. It has been observed that the change in lattice strain significantly changes the electron band structure of the semiconductor and improve the photocatalytic performance.

The photocatalytic activities of as-prepared $BiVO_4$ nanorods, ZnCdS nanoparticles and $BiVO_4$–ZnCdS heterostructure samples were evaluated for the production of hydrogen from water splitting under visible light irradiation. Catalysts were dispersed in aqueous Na_2S and Na_2SO_3 solutions, which act as sacrificial agents to scavenge the photogenerated holes and alleviate the electron-hole pair recombination while maintaining the stability of the catalyst [49]. Fig. 6A displays the photocatalytic hydrogen production curves of as-prepared catalysts, indicating a linear progression of hydrogen production with irradiation time. Bare $BiVO_4$ nanorods are practically inactive for hydrogen production and does not show any photocatalytic activity under visible light irradiation because the photogenerated electron in the $BiVO_4$ conduction band has the potential to reduce oxygen into hydrogen

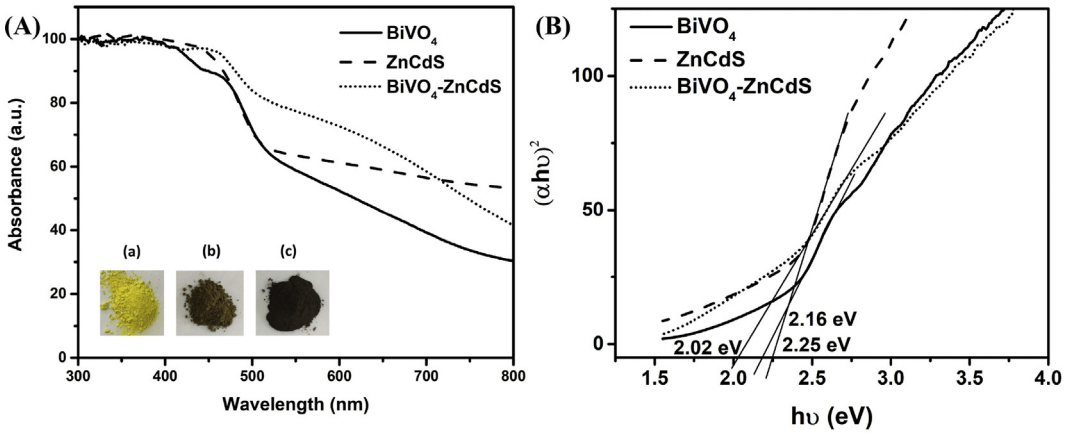

Fig. 5 – UV–visible diffuse reflectance spectra (A) and corresponding *Tauc* plot (B) for $BiVO_4$, ZnCdS and $BiVO_4$–ZnCdS; the inset are the digital photographs of ZnCdS (a), $BiVO_4$ (b) and $BiVO_4$–ZnCdS heterostructure (c).

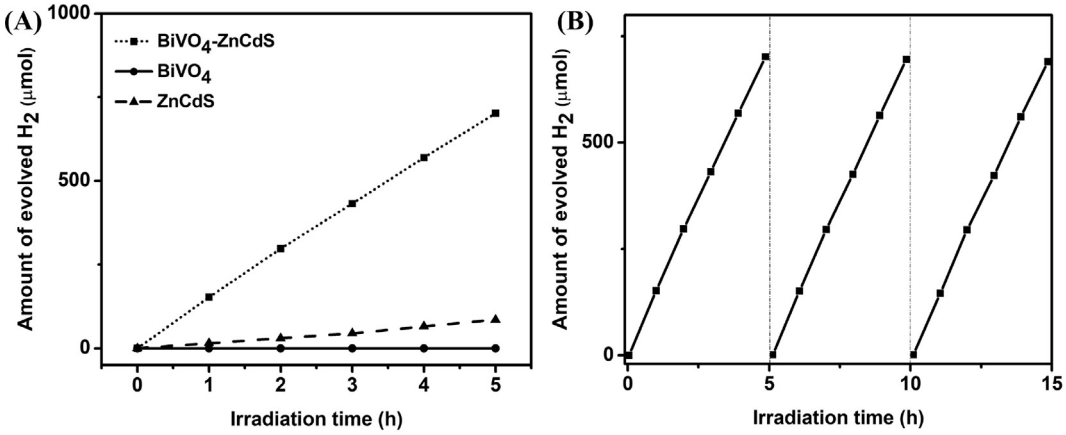

Fig. 6 – Time courses of photocatalytic H_2 evolution from water splitting on $BiVO_4$ nanorods, ZnCdS nanoparticles and $BiVO_4$–ZnCdS heterostructure under visible–light illumination ($\lambda \geq 420$ nm) (A). Time courses of photocatalytic H_2 evolution from water solution on $BiVO_4$–ZnCdS heterostructure (B).

peroxide but cannot reduce water into hydrogen due to low conduction band position [50]. ZnCdS nanoparticles on the other hand exhibited some photocatalytic activity (15 μmol g^{-1} h^{-1}). Despite the low band gap and ideal conduction band position of ZnCdS, the low photocatalytic performance mainly ascribed to the intrinsic characteristic of CdS to fast recombination of charge carrier and photocorrosion behavior [51]. However, after combining ZnCdS with $BiVO_4$ nanorods and heat treatment at 400 °C, the hydrogen production rates were drastically enhanced (152.5 μmol g^{-1} h^{-1}). The performance reached a level of 702.3 μmol after 5 h of irradiation strongly indicating the structural advantage of $BiVO_4$–ZnCdS heterostructure in promoting the photocatalytic activities. The effect of calcination temperature on photocatalytic H_2 production have been studied previously and it was observed that, 400 °C was the optimum temperature with highest photocatalytic hydrogen production rate compared to without calcination or at lower/higher temperatures [35]. The change in photocatalytic performance with respect to calcination temperature was largely influenced due to change in crystallinity, surface area, sintering and interface contact. At lower temperature, the intimate contact between two photocatalysts cannot be formed resulting in lower electron transfer while at higher temperature the agglomeration of nanoparticles reduces the available surface area for photocatalytic reaction resulting in lower performance. Moreover, mixed phases of $BiVO_4$ can efficiently avail the transfer of electrons compared with tetragonal or monoclinic phase [38]. At higher temperature, $BiVO_4$ change to monoclinic geometry which negatively affect its photocatalytic performance. The significantly enhanced activity of $BiVO_4$–ZnCdS heterostructure compared to bare samples suggested an important synergistic link between intimately contacted $BiVO_4$ nanorods and ZnCdS nanoparticles after heat treatment at 400 °C. The stability of $BiVO_4$–ZnCdS up to three consecutive cycles for photocatalytic H_2 production was also assessed. As shown in Fig. 6B, the $BiVO_4$–ZnCdS heterostructure does not exhibit any obvious decrease in photocatalytic activity, suggesting the excellent stability of the as-obtained heterostructure. The photocatalytic H_2 production rate at 5 h after three consecutive cycles shows a small decrease (690.67 μmol g^{-1} h^{-1}) compared to initial value (702.3 μmol g^{-1} h^{-1}). Moreover, XRD analysis after three stability cycles was also performed and no

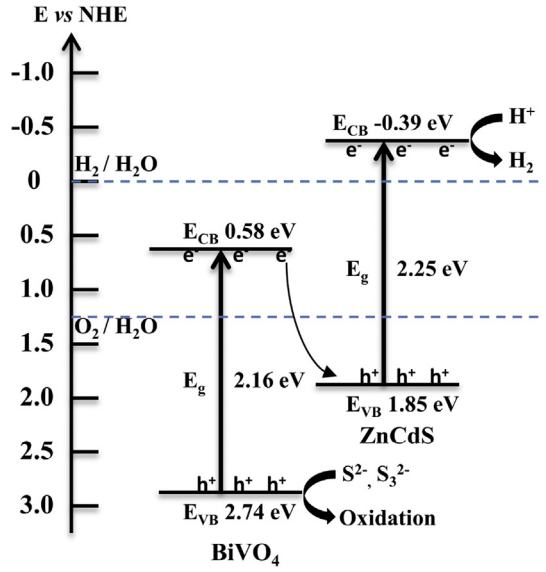

Fig. 7 – A schematic diagram illustrating the band positions and charge transfer process for $BiVO_4$–ZnCdS heterostructure.

change in crystal structure was observed indicating the excellent stability of $BiVO_4$–ZnCdS heterostructure (Fig. S2).

To access the mechanism for enhanced photocatalytic hydrogen production over $BiVO_4$–ZnCdS heterostructure, the energy band alignments of ZnCdS nanoparticles and $BiVO_4$ nanorods were also calculated. The conduction and valence band potentials of a photocatalyst can be calculated by following equations [52,53]:

$$E_{VB} = X - E_e + 0.5E_g \quad (1)$$

$$E_{CB} = E_{VB} - E_g \quad (2)$$

where, E_{VB} and E_{CB} are the valence and conduction band potentials, respectively, E_g is the band-gap energy, E_e is the energy of the free electrons on the hydrogen scale and X is the absolute electronegativity. From Equations (1) and (2), the conduction and valence band potentials were obtained for ZnCdS nanoparticles ($E_{VB} = 1.85$ eV, $E_{CB} = -0.39$ eV) and $BiVO_4$ nanorods ($E_{VB} = 2.74$ eV, $E_{CB} = 0.58$ eV). The band energy diagrams for ZnCdS and $BiVO_4$ were depicted in Fig. 6 and results confirm that $BiVO_4$–ZnCdS can form an overlapping band structure. As shown in Fig. 7, the conduction band of $BiVO_4$ is higher than the valence band of ZnCdS but lower than the potential required for hydrogen evolution, which was the reason of no photocatalytic hydrogen production over $BiVO_4$ nanorods. The ZnCdS nanoparticles showed some water splitting capabilities for the production of hydrogen which implies to the low band gap values and suitable conduction band position. But the lower values may be ascribed to the fast recombination of electron-hole pairs. $BiVO_4$–ZnCdS heterostructure on the other hand shows highest hydrogen production among studied catalysts which strongly implied the construction of a Z-scheme system [28]. The Z-scheme

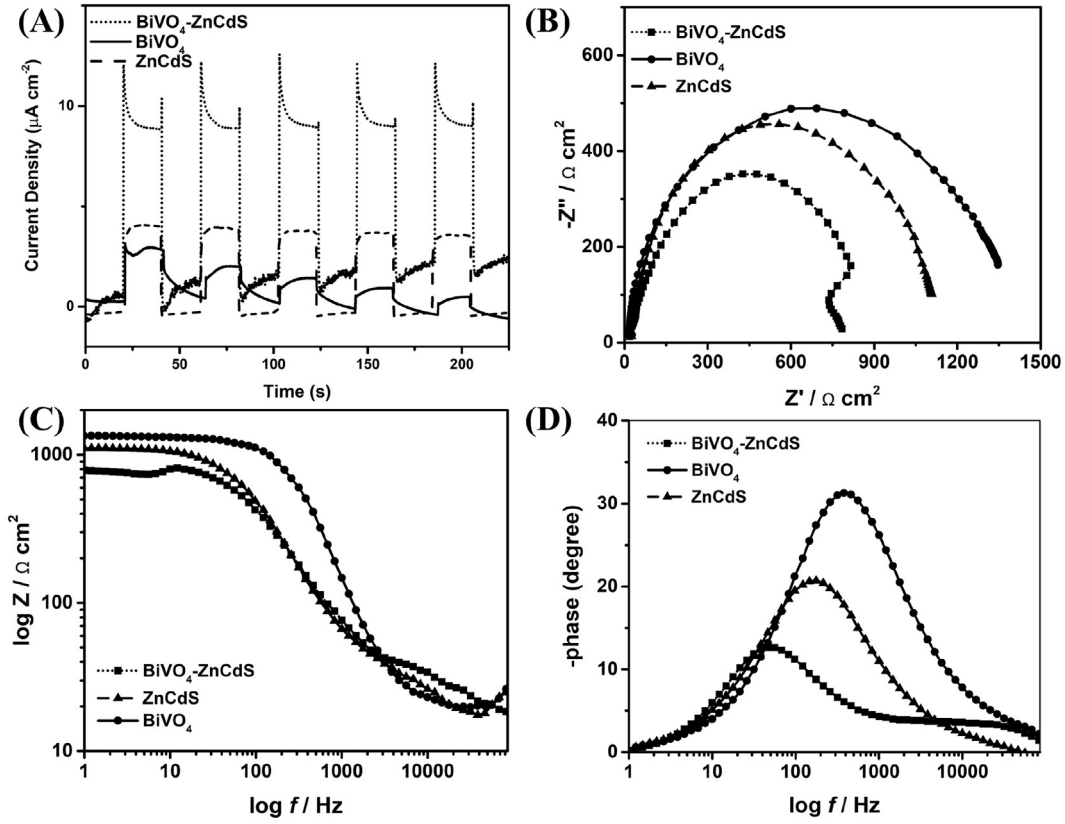

Fig. 8 – Photocurrent response vs. time for $BiVO_4$, ZnCdS and $BiVO_4$–ZnCdS heterostructure (λ ≥ 420 nm) (A); EIS curves of $BiVO_4$, ZnCdS and $BiVO_4$–ZnCdS heterostructure and corresponding bode plot (B-D).

electron transfer pathway needs to satisfy three conditions; i.e., Photosystem-I can only produce O_2, Photosystem-II can only produce H_2 and overall water splitting can occur in the presence of both. $BiVO_4$ photocatalyst have been reported to produce O_2, while $Zn_{1-x}Cd_xS$ have also shown potential to be used for photocatalytic H_2 production. Our results also showed that the $BiVO_4$ nanorods were not able to produce H_2 indicating lower band gap position while ZnCdS nanoparticles alone showed some H_2 production. After forming heterostructure, the rate of photocatalytic H_2 production increased drastically which indicates that the photogenerated electrons in conduction band of $BiVO_4$ nanorods tend to recombine with holes in valence band of ZnCdS, while photogenerated electron of ZnCdS implies to hydrogen production. This is consistent with the Z-scheme electron transfer pathway [54].

To further illustrate the well-maintained Z-scheme pathway, the formation and migration of photogenerated charge carriers over pure $BiVO_4$ nanorods, ZnCdS nanoparticles and $BiVO_4$–ZnCdS heterostructure were investigated using photoelectrochemical tests under visible-light irradiation ($\lambda \geq 420$ nm). The transient photocurrent response of semiconductors under light switch on/off can be used as a method to understand the charge separation ability [55]. It can be seen from Fig. 8A that the photocurrent response of bare $BiVO_4$ nanorods and ZnCdS nanoparticles is very low strongly suggesting the fast recombination of electron-hole pairs which hindering their widespread application for solar water splitting [56]. However, the transient photocurrent values for $BiVO_4$–ZnCdS heterostructure were much higher compared to bare samples indicating higher charge separation efficiency while reducing surface recombination. The higher photocurrent response further strengthens the proposed Z-scheme interface electron transfer for water splitting which is responsible for enhanced photocatalytic hydrogen production. The electron in the conduction band can be efficiently consumed by the holes at the valence band of ZnCdS resulting in higher photocurrent abilities and charge separation. Moreover, electrochemical impedance spectroscopy (EIS) was also used to determine the contribution of the independent components to the electrochemical properties of $BiVO_4$–ZnCdS heterostructure. The arc radius of the semicircular part of the Nyquist plot shows the surface reaction rate and electrode resistance. It has been previously observed that, the smaller the radius of the arc, the easier the charge transfer efficiency from the catalyst to the electrolyte solution [57]. As displayed in Fig. 8B, $BiVO_4$–ZnCdS heterostructure presented a smaller arc radius of the Nyquist plot compared with $BiVO_4$ nanorods and ZnCdS nanoparticles, suggesting an effective charge separation. Fig. 8C and D also shows the corresponding bode plots that reflect the efficient electron lifetime of $BiVO_4$–ZnCdS heterostructure. The characteristic peak frequency shifts to the lower value for $BiVO_4$–ZnCdS compared to bare $BiVO_4$ and ZnCdS implying longer electron lifetime which can be attributed to the reduced recombination process, resulting in accelerating electron transfer, increasing electron density, and improving photocatalytic H_2 production. Overall, results conclude that $BiVO_4$–ZnCdS heterostructure showed promising performance for photocatalytic H_2 production due to improved visible light absorption efficiency, reduced recombination rate including charge transportation, and enhanced photoelectron collection process.

Conclusion

In this work, $BiVO_4$ nanorods were successfully synthesized and used as support to anchor ZnCdS nanoparticles forming a $BiVO_4$–ZnCdS heterostructure. The heterostructure catalyst was well characterized through high-resolution transmission electron microscope, EDX elemental mapping, X-ray diffraction and X-ray photoelectron spectroscopic analysis. The UV–vis diffuse reflectance spectra showed stronger optical properties for $BiVO_4$–ZnCdS heterostructure compared to bare samples and subsequent band gap calculations and band alignment studies confirm the Z-scheme pathway for electron movement through interfacial contact. The $BiVO_4$–ZnCdS heterostructure showed 10 times higher hydrogen production rates from water splitting compared to ZnCdS while $BiVO_4$ nanorods does not show any activity due to its low conduction band position for water splitting. The enhanced performance of $BiVO_4$–ZnCdS heterostructure was further studied through transient photocurrent response curves and electrochemical impedance spectroscopy, which shows efficient transfer of electrons at the interface to achieve improved separation of the photogenerated electrons and holes and easier charge transfer efficiency from the catalyst to the electrolyte solution which resulted in higher photocatalytic hydrogen production.

Declaration of competing interest

The authors declare the following financial interests/personal relationships which may be considered as potential competing interests. Peter Kasak, corresponding author, on behalf of all authors.

Acknowledgement

This publication was supported by Qatar University Grant QUCG-CAM-22/23-504. The authors also acknowledge financial support from USTC/Anhui Government Scholarships programme and CAS-TWAS President's Fellowship programme. The finding achieved herein is solely the responsibility of the authors.

Appendix A. Supplementary data

Supplementary data to this article can be found online at https://doi.org/10.1016/j.ijhydene.2021.12.193.

REFERENCES

[1] Lewis NS, Nocera DG. Powering the planet: chemical challenges in solar energy utilization. Proc Natl Acad Sci Unit States Am 2006;103:15729e35.
[2] Furat D, Martin A, Shafiullah GM. Hydrogen production for energy: an overview. Int J Hydrogen Energy 2020;45:3847–69.

[3] Fujishima A, Honda K. Electrochemical photolysis of water at a semiconductor electrode. Nature 1972;238:37–8.
[4] Zhiliang J, Yanbing L, Xuqiang H. Ni, Co-based selenide anchored g-C_3N_4 for boosting photocatalytic hydrogen evolution. Acta Phys Chim Sin 2021;37(10):1912033.
[5] Chen XB, Shen SH, Guo LJ, Mao SS. Semiconductor-based photocatalytic hydrogen generation. Chem Rev 2010;110:6503–70.
[6] Turner JA. Sustainable hydrogen production. Science 2004;305:972–4.
[7] Rodriguez CA, Modestino MA, Psaltis D, Moser C. Design and cost considerations for practical solar-hydrogen generators. Energy Environ Sci 2014;7:3828e35.
[8] Zou ZG, Ye JH, Sayama K, Arakawa H. Direct splitting of water under visible light irradiation with an oxide semiconductor photocatalyst. Nature 2001;414:625–7.
[9] Kato H, Asakura K, Kudo A. Highly efficient water splitting into H_2 and O_2 over lanthanum-doped $NaTaO_3$ photocatalysts with high crystallinity and surface nanostructure. J Am Chem Soc 2003;125:3082–9.
[10] Acar C, Dincer I, Naterer GF. Review of photocatalytic water-splitting methods for sustainable hydrogen production. Int J Energy Res 2016;40:1449–73.
[11] Matsuoka M, Kitano M, Takeuchi M, Tsujimaru K, Anpo M, Thomas JM. Photocatalysis for new energy production: recent advances in photocatalytic water splitting reactions for hydrogen production. Catal Today 2007;122:51–61.
[12] Kudo A. Recent progress in the development of visible light-driven powdered photocatalysts for water splitting. Int J Hydrogen Energy 2007;32:2673–8.
[13] Zhimin J, Qing C, Qiaoqing Z, Rongchen S, Peng Z, Xin Li. Constructing 1D/2D Schottky-based heterojunctions between $Mn_{0.2}Cd_{0.8}S$ nanorods and Ti_3C_2 nanosheets for boosted photocatalytic H_2 evolution. Acta Phys Chim Sin 2021;37(6):2010059.
[14] Yang L, Xuqiang H, Haiqiang H, Zhiliang J. High efficiency electron transfer realized over $NiS_2/MoSe_2$ S-scheme heterojunction in photocatalytic hydrogen evolution. Acta Phys Chim Sin 2021;37(6):2008030.
[15] Ashwin-Kishore MR, Karin L, Ponniah R. Two-Dimensional CdX/C_2N (X = S, Se) heterostructures as potential photocatalysts for water splitting: a dft study. ACS Omega 2020;5(37):23762–8.
[16] Ziyu L, Teng Y, Chenxu H, Kwang-Leong C, Chaozong L. Thermodynamic and kinetics of hydrogen photoproduction enhancement by concentrated sunlight with CO2 photoreduction by heterojunction photocatalysts. Energy and AI 2021;6:100102.
[17] Wang YB, Wang YS, Xu R. Photochemical deposition of Pt on CdS for H_2 evolution fromwater: markedly enhanced activity by controlling Pt reduction environment. J Phys Chem C 2013;117:783e90.
[18] Zong X, Yan HJ, Wu GP, Ma GJ, Wen FY, Wang L, et al. Enhancement of photocatalytic H_2 evolution on CdS by loading MoS_2 as cocatalyst under visible light irradiation. J Am Chem Soc 2008;130:7176e7.
[19] Jiang DC, Sun ZJ, Jia HX, Lu DP, Du PW. A cocatalyst-free CdS nanorod/ZnS nanoparticle composite for high-performance visible-light-driven hydrogen production from water. J Mater Chem 2016;4:675e83.
[20] Dai Y, Yin L. Low Fe-doped Bi_2O_3 Photocatalyst with long wavelength response: crystalline transition and mechanisms by first calculation. J Alloys Compd 2013;563:80e4.
[21] Zhang L, Wang W, Yang J, Chen Z, Zhang W, Zhou L, et al. Sonochemical synthesis of nanocrystallite Bi_2O_3 as a visiblelight-driven photocatalyst. Appl Catal A Gen 2006;308:105.
[22] Weckhuysen BM, Keller DE. Chemistry, spectroscopy and the role of supported vanadium oxides in heterogeneous catalysis. Catal Today 2003;78:25–46.
[23] Thangavelu P, Le S, Gangaiah M, Dalavar HA, Renyan L, Krishna PK, Pascal ES, Peng W. Vastly enhanced $BiVO_4$ photocatalytic OER performance by NiCoO2 as cocatalyst. Adv Mater Interfac 2017;4:1700540.
[24] Malathi A, Madhavan J, Muthupandian A, Prabhakarn A. A review on $BiVO_4$ photocatalyst: activity enhancement methods for solar photocatalytic applications. Appl Catal A-Gen 2018;555:47–74.
[25] Cheng J, Yan X, Mo Q, Liu B, Wang J, Yang X, Li L. Facile synthesis of g-$C_3N_4/BiVO_4$ heterojunctions with enhanced visible light photocatalytic performance. Ceram Int 2017;43:301–7.
[26] Xu S, Fu D, Song K, Wang L, Yang Z, Yang W, Hou H. One-dimensional $WO_3/BiVO_4$ heterojunction photoanodes for efficient photoelectrochemical water splitting. Chem Eng J 2018;349:368–75.
[27] Sahar M, Rym A, Erika S, Semy BC, Noelia Ma, Rufino M, Navarro Y, José LGF, Saïd Z. Pt–$BiVO_4/TiO_2$ composites as Z-scheme photocatalysts for hydrogen production from ethanol: the effect of $BiVO_4$ and Pt on the photocatalytic efficiency. New J Chem 2021;45:4481–95.
[28] Zhou P, Yu J, Jaroniec M. All-solid-state Z-scheme photocatalytic systems. Adv Mater 2014;26:4920–35.
[29] Hideyuki K, Yusuke T, Tohru S, Satoshi K. Z-scheme photocatalytic hydrogen production over WO_3/g-C_3N_4 composite photocatalysts. RSC Adv 2014;4:21405e9.
[30] Fangshu X, Chuchu C, Jingwen Z, Qiuwen L, Cheng C, Caijin H. Tunable charge transfer efficiency in H_xMoO_3@$ZnIn_2S_4$ hierarchical direct Z-scheme heterojunction toward efficient visible-light-driven hydrogen evolution. Appl Catal B Environ 2021;285:119818.
[31] Han VDang, Yen HW, Jeffrey CSW. Z-scheme photocatalyst Pt/GaP-TiO_2-SiO_2:Rh for the separated H_2 evolution from photocatalytic seawater splitting. Appl Catal B Environ 2021;296:120339.
[32] Che Y, Lu B, Qi Q, et al. Bio-inspired Z-scheme g-C_3N_4/Ag_2CrO_4 for efficient visible-light photocatalytic hydrogen generation. Sci Rep 2018;8:16504.
[33] Xuesong Z, Yingying Y, Shaobin H, Yixiao W, Yiyang M, Guan Z, Zhenghua Z. Z-scheme photocatalytic production of hydrogen peroxide over $Bi_4O_5Br_2/g$-C_3N_4 heterostructure under visible light. Appl Catal B Environ 2020;278:119251.
[34] Xing F, Liu Q, Huang C. Mo-doped $ZnIn_2S_4$ flower-like hollow microspheres for improved visible light-driven hydrogen evolution. Sol RRL 2020;4:1900483.
[35] Imran M, Yousaf AB, Kasak P, Zeb A, Zaidi SJ. Highly efficient sustainable photocatalytic Z-scheme hydrogen production from an α-Fe_2O_3 engineered ZnCdS heterostructure. J Catal 2017;353:81–8.
[36] Shrabani G, Samrat S, Bikram KD, Dipayan S, Madhupriya S, Kalyan KC. Band edge tuned $Zn_xCd_{1-x}S$ solid solution nanopowders for efficient solar photocatalysis. Phys Chem Chem Phys 2017;19:29998–30009.
[37] Sleight AW, Chen HY, Ferretti A, Cox DE. Crystal growth and structure of $BiVO_4$. Mater Res Bull 1979;14(12):1571–81.
[38] Wenjuan L, Xiao W, Ze W, Yi M, Xiaolan S, Tingjiang Y, Jinmao Y, Desheng K. Relationship between crystalline phases and photocatalytic activities of $BiVO_4$. Mater Res Bull 2016;83:259–67.
[39] Ruishi X, Zhicheng G, Xuhai L, Haifeng L, Hongjuan S, Baogang G, Qinghua L, Yuanli L. Rational manipulation of lattice strain to tailor the electronic and optical properties of nanostructures. Ceram Int 2021;47(22):31476–84.
[40] Thangavelu P, Le S, Gangaiah M, Dalavar HA, Renyan L, Krishna PK, Pascal ES, Peng W. Vastly enhanced $BiVO_4$

photocatalytic OER performance by $NiCoO_2$ as cocatalyst. Adv Mater Interfac 2017;4:1700540.
[41] Xu X, Lu RJ, Zhao XF, Zhu Y, Xu SL, Zhang FZ. Novel mesoporous ZnxCd1_xS nanoparticles as highly efficient photocatalysts. Appl Catal B Environ 2012;125:11.
[42] Samapti K, Biswarup S, Tanusree K, Swapan KP. Microstructure characterization of hydrothermally synthesized PANI/$V_2O_5 \cdot nH_2O$ heterojunction photocatalyst for visible light induced photodegradation of organic pollutants and non-absorbing colorless molecules. J Hazard Mater 2017;339:161–73.
[43] Wei Z, Ying L, Zhongbo W, Shaogui Y, Huan H, Cheng S. Fabrication of a novel p-n heterojunction photocatalyst n-$BiVO_4$@p-MoS_2 with core-shell structure and its excellent visible-light photocatalytic reduction and oxidation activities. Appl Catal B Environ 2016;185:242–52.
[44] Sun SM, Wang WZ, Zhang L, Zhou L, Yin WZ, Shang M. Visible light-induced efficient contaminant removal by Bi_5O_7I. Environ Sci Technol 2009;43:2005–10.
[45] Meysam T, Byeong-Kyu L. Recent advances in $BiVO_4$ semiconductor materials for hydrogen production using photoelectrochemical water splitting. Renew Sustain Energy Rev 2019;111:332–43.
[46] Wang ZS, Yang XD, Jia HX, Wang YQ. Preparation of self-assembled hollow microsphere CdS via solvothermal method and its optical properties. J Mater Sci Mater Electron 2016;27:9725–33.
[47] Walash A, Yan Y, Huda MH, Al-Jassim MM, Wei SH. Band edge electronic structure of $BiVO_4$: elucidating the role of the Bi s and V d orbitals. Chem Mater 2009;21:547–51.
[48] Qin L, Huan M, Peng Z, Yingqiu Z, Juan W, Jiaguo Y, JianRu G. $Zn_{1-x}Cd_xS$ solid solutions with controlled bandgap and enhanced visible-light photocatalytic H_2-production activity. ACS Catal 2013;3:882–9.
[49] Maeda K. Z-scheme water splitting using two different semiconductor photocatalysts. ACS Catal 2013;3:1486–503.
[50] Ren L, Jiabin R, Dian Z, Jiqiang N, Ziyang Z, Yongjiang W, Yijun Z, Changcheng Z, Yong H. Band-gap engineering of porous $BiVO_4$ nanoshuttles by Fe and Mo co-doping for efficient photocatalytic water oxidation. Inorg Chem Front 2017;4:2045–54.
[51] Zong X, Wu GP, Yan HJ, Ma GJ, Shi JY, Wen FY, Wang L, Li C. Photocatalytic H_2 evolution on MoS_2/CdS catalysts under visible light irradiation. J Phys Chem C 2010;114:1963–8.
[52] Butler MA, Ginley D. Ginley, prediction of flatband potentials at semiconductor-electrolyte interfaces from atomic electronegativities. J Electrochem Soc 1978;125:228–32.
[53] Kim YI, Atherton SJ, Brigham ES, Mallouk TE. Sensitized layered metal oxide semiconductor particles for photochemical hydrogen evolution from nonsacrificial electron donors. J Phys Chem 1993;97:11802–10.
[54] Quanlong X, Liuyang Z, Jiaguo Y, Swelm W, Ahmed A, Mietek J. Direct Z-scheme photocatalysts: principles, synthesis, and applications. Mater Today 2018;21:1042–63.
[55] Phu ND, Hoang LH, Vu PK, Kong MH, Chen XB, Wen HC, Chou WC. Control of crystal phase of $BiVO_4$ nanoparticles synthesized by microwave assisted method. J Mater Sci Mater Electron 2016;27:6452–6.
[56] Gao X, Wu HB, Zheng L, Zhong Y, Hu Y, Lou XW. formation of mesoporous heterostructured $BiVO_4$/Bi_2S_3 hollow discoids with enhanced photoactivity. Angew Chem Int Ed 2014;53:5917–21.
[57] Wei ZH, Wang YF, Li YY, Zhang L, Yao HC, Li ZJ. Enhanced photocatalytic CO_2 reduction activity of Z-scheme CdS/$BiVO_4$ nanocomposite with thinner $BiVO_4$ nanosheets. J CO_2 Util 2018;28:15–25.